Structural Engineering and Mechanics, *Vol. 72, No. 2 (2019) 169-180*
DOI: https://doi.org/10.12989/sem.2019.72.2.169

Wake-induced vibration of the hanger of a suspension bridge: Field measurements and theoretical modeling

Shouying Li*[1], Yangchen Deng[1], Xu Lei[1], Teng Wu[2] and Zhengqing Chen[1]

[1]*Key Laboratory for Wind and Bridge Engineering of Hunan Province, College of Civil Engineering, Hunan University, Changsha 410082, China*
[2] *Department of Civil, Structural and Environmental Engineering, University at Buffalo, Baffalo, NY 14260, USA*

(Received March 7, 2019, Revised May 5, 2019, Accepted May 23, 2019)

Abstract. The underlying mechanism of the wind-induced vibration of the hangers of the suspension bridges is still not fully understood at present and hence is comprehensively examined in this study. More specifically, a series of field measurements on the No. 2 hanger of the Xihoumen Bridge was first carefully conducted. Large amplitude vibrations of the hanger were found and the oscillation amplitude of the leeward cable was obviously larger than that of the windward cables. Furthermore, the trajectory of the leeward cable was close to an ellipse, which agreed well with the major characteristics of wake-induced vibration. Then, a theoretical model for the wake-induced vibration based on a 3-D continuous cable was established. To obtain the responses of the leeward cable, the finite difference method (FDM) was adopted to numerically solve the established motion equation. Finally, numerical simulations by using the structural parameters of the No. 2 hanger of the Xihoumen Bridge were carried out within the spatial range of $4\leq X\leq 10$ and $0\leq Y\leq 4$ with a uniform interval of $\Delta X=\Delta Y=0.25$. The results obtained from numerical simulations agreed well with the main features obtained from the field observations on the Xihoumen Bridge. This observation indicates that the wake-induced vibration might be one of the reasons for the hanger oscillation of the suspension bridge. In addition, the effects of damping ratio and windward cable movement on the wake-induced vibration of the leeward cable were numerically investigated.

Keywords: hangers of suspension bridges; wake-induced vibration; field measurements; theoretical analyses; structural damping

1. Introduction

The length of hangers of the suspension bridge increases with the bridge span. Since the hanger tension is passively produced only by the gravity of the deck and the external loadings acting on the deck, the natural frequency of the hanger is far lower than that of the prestressed stay cable. Hence, the hanger of suspension bridge is sensitively prone to wind-induced vibrations. Serious and long-lasting vibration of the hanger will change the mechanical properties of bridge structure and then cause fatigue problem and impair the safety and serviceability of the whole bridge (Greco *et al*. 2013, Lonetti and Pascuzzo 2014). There are a number of hanger vibrations reported in the literature, for example, the Akashi-Kaikyo Bridge in Japan (Fujino *et al*. 2012), the Great Belt East Bridge in Denmark (Laursen *et al*., 2005) and the Xihoumen Bridge in China (Hua *et al*. 2019; Wen *et a*l. 2018). However, it seems that the researchers have different opinions about the underlying mechanism of the hanger vibration. Laursen *et al*. (2005) speculated that the ice accretions might lead to the vibration of the hanger based on a field observation on the Great Belt East Bridge. Zhang *et al*. (2016) proposed that the vibration of the main cable could result in large amplitude vibration of the hangers near the pylon based on a numerical analysis for the Xihoumen Bridge. Li *et al*. (2017) and Chen *et al*. (2018) both found that the wake of the pylon could lead to large amplitude vibration of the hangers. Wen *et al.* (2018) and Hua *et al.* (2019) conducted a series of wind tunnel tests and studied aerodynamic interference of quadruple cables of the Xihoumen Bridge and verified the efficiency of spacers on suppress the wake-induced vibration through field measurements. Li *et al.* (2019) and Deng *et al*. (2019a) respectively established quasi-steady and unsteady 2-D theoretical models and found that the hanger vibration could be induced by the aerodynamic interference between the cables of a hanger (wake-induced vibration).

In the past few decades, the features of the wake-induced vibration of two circular cylinders have been widely investigated. Some researchers focused on the flow patterns around two circular cylinders. For example, Igarashi (1981, 1984) investigated the flow patterns of two tandem circular cylinders and proposed that there are eight types of flow patterns around two tandem circular cylinders. Zdravkovich (1987) classified the flow patterns of two tandem circular cylinders into three basic regimes: the extended-body regime, the reattachment regime and the co-shedding regime. Gu and Sun (1999) studied the flow patterns of two staggered circular cylinders by utilizing pressure measurement and flow visualization methods and put forward that there are three different types of flow patterns: the wake interference, the shear layer interference and the neighborhood interference. Sumner *et al*. (2000)

*Corresponding author, Professor
E-mail: shyli@hnu.edu.cn

ISSN: 1225-4568 (Print), 1598-6217 (Online)

further investigated a much wider range of flow field for two staggered circular cylinders and identified nine different flow patterns. The aerodynamic forces of two tandem and staggered circular cylinders could be obtained by means of wind tunnel tests (Arie *et al*., 1983; Zhang and Melbourne, 1992; Alam *et al*., 2003; Sumner and Richards, 2003; Akosile and Sumner, 2003; Sumner *et al*., 2005) and these data is the basis of further theoretical studies. On the other hand, Kim *et al.* (2009) experimentally investigated the characteristics of the wake-induced vibration of two tandem circular cylinders with L/D=0.1-3.2 (L is center-to-center distance between two cylinders and D is the cylinder diameter). Yagi *et al*. (2015) carried out wind tunnel tests to identify the derivatives of the leeward cylinder and conducted a series of flutter analyses to obtain the responses of the wake-induced vibration. Recently, more detailed parametric studies about the responses of the wake-induced vibration, including the effects of diameter ratio, natural frequency and surface roughness, were accomplished by Assi (2014), Qin *et al*. (2018) and Du *et al*. (2017). A number of researchers made great efforts to reveal the underlying mechanism of wake-induced vibration. Assi *et al.* (2010, 2013) conducted experiments in a water flume on a pair of cylinders in tandem arrangement and concluded that the downstream cylinder is excited by the unsteady vortex-structure interactions between the body and the upstream wake. Mysa *et al.* (2016, 2017) numerically investigated the origin of wake-induced vibration of two tandem circular cylinders and have reached similar mechanism as Assi *et al.* (2010, 2013). Deng *et al.* (2019) theoretically investigated the wake-induced vibration and concluded that the negative aerodynamic stiffness is the main cause of wake-induced vibration.

At present, the mechanisms of wake-induced vibration of transmission lines and offshore risers have been extensively studied (Païdoussis *et al*. 2011). However, very few efforts have been made towards the mechanism of wake-induced vibration of the hangers of suspension bridges. Few results obtained from field observations were reported. Furthermore, only 2-D theoretical models, which are much different from the 3-D prototype cable, have been established to explain the mechanism of wake-induced vibration of the hangers. In the present study, the underlying mechanism of the hanger vibration is comprehensively investigated. More specifically, a series of field measurements on the No. 2 hanger of the Xihoumen Bridge was first conducted. Then, a theoretical model for the wake-induced vibration based on a 3-D continuous cable was established to obtain the responses of the leeward cable. The numerical results of wake-induced hanger vibration were carefully compared to those from field measurements.

1. Field measurements on the hangers of the Xihoumen bridge

A series of field measurements on the No. 2 hanger of the Xihoumen Bridge were conducted to obtain its wind-induced responses. The Xihoumen Bridge, which has a 1650-meter-long main span and a 578-meter-long side span,

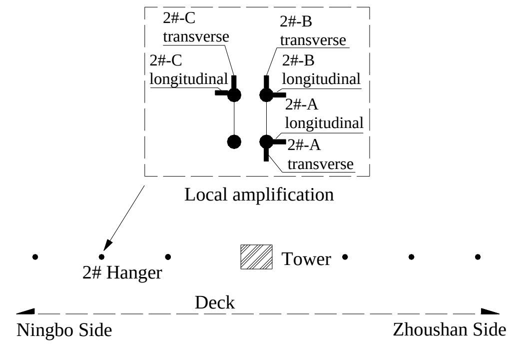

Fig. 1 Arrangement of the six accelerometers

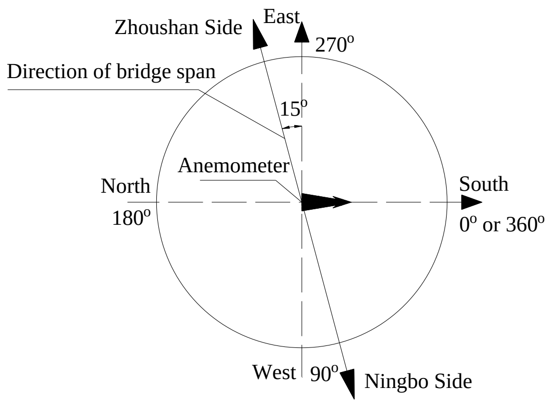

Fig. 2 Definition of wind direction

is located between Ningbo City and Zhoushan Island in the eastern China. The No. 2 hanger at the side span of the Xihoumen Bridge was found to oscillate violently during the operation stage, therefore, was selected for the field measurements. The No. 2 hanger consists of four cables, which has the center-to-center spacing of 300mm in the longitudinal direction of the bridge and 600mm in transverse direction, respectively. The diameter of the cable is 88 mm. Six accelerometers were installed on the Cables A, B and C of the No. 2 hanger at the height of 15m over the bridge deck. The sampling frequency of the accelerometers is 10Hz. The wind velocity and the corresponding wind direction were collected by an anemometer installed at the height of 4m over the bridge deck. The sampling frequency of the anemometer is 1Hz. The arrangement of the six accelerometers is shown in Fig.1 and the definition of wind direction is shown in Fig.2. Figure 3 presents the photos of the accelerometers and the anemometer installed on the No. 2 hanger.

Obvious oscillation of the cables on the leeward side was found at the wind velocity of 5-8 m/s, while the windward cables only vibrates slightly. Two typical data sets, including acceleration on the cables, the wind velocity and the wind direction, are presented in the present study. The first is collected from 0:00 to 24:00 on January 14, 2014 (as shown in Fig.4) and is named Data 1 in the following contents. The second is collected from 0:00 to 24:00 on January 26, 2014 (as shown in Fig.5) and is named Data 2. It could be found from Fig.4 that the hanger oscillates obviously between 18:00-22:00 and the corresponding mean wind velocity and direction are respectively about 6m/s and 170°. Noted that wind direction of 170° signifies that the wind is nearly perpendicular to the beam of the bridge, as shown in Fig.4 (c) and (d). The peak acceleration of Cable A in the longitudinal direction, which is about 10 m/s^2, is obviously larger than those of Cables B and C. However, in the transverse direction, the difference between the peak accelerations of Cables A, B and C is not as obvious as that in the longitudinal direction. From Fig.5, it is found that the responses of Cables A, B and C are similar to those in Fig.4. It seems that the violent vibration of Cable A is related to the wake induced by Cables B and C and this indicates the No. 2 hanger of the Xihoumen Bridge may have suffered wake-induced vibration.

(a)Accelerometers

(b) Anemometer

Fig. 3 Photos of the accelerometers and anemometer installed on the hanger

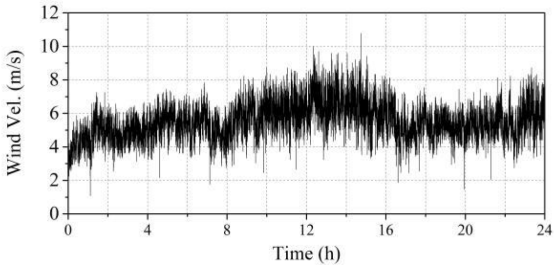

(a) Wind velocity

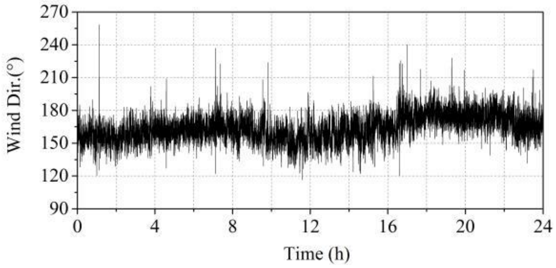

(b) Wind direction

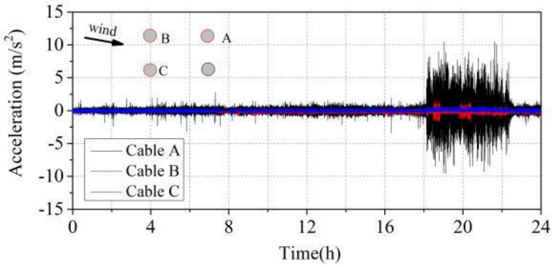

(c) Acceleration of cables in longitudinal direction

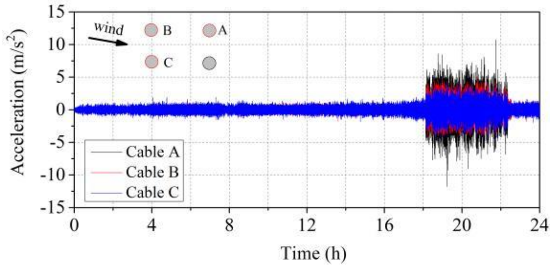

(d) Acceleration of cables in transverse direction

Fig. Data 1: January 14, 2014

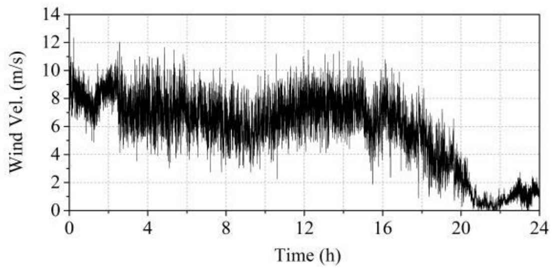

(a) Wind velocity

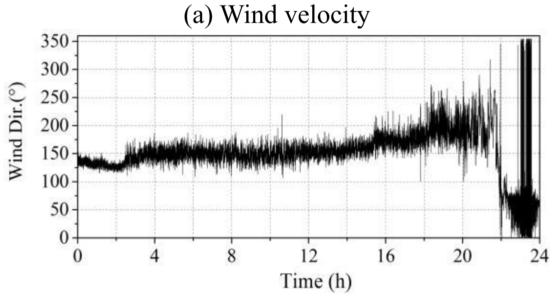

(b) Wind direction

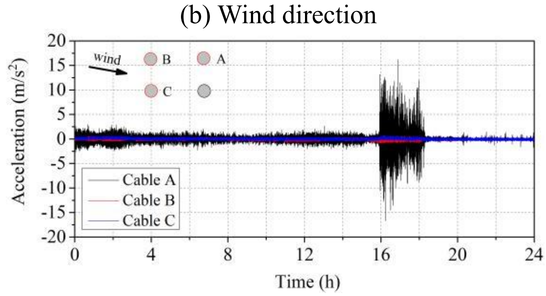

(c) Acceleration of cables in longitudinal direction

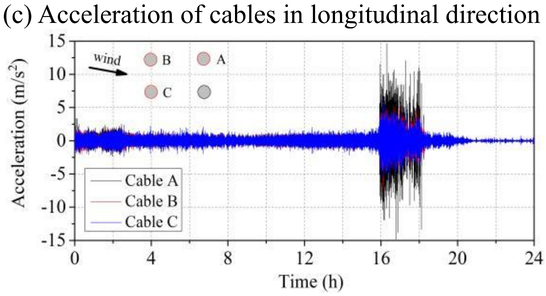

(d) Acceleration of cables in transverse direction

Fig. 5 Data 2: January 26, 2014

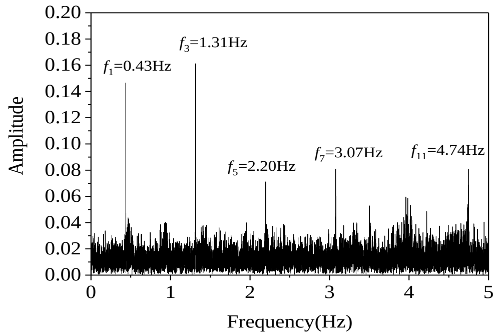

(a) Data 1

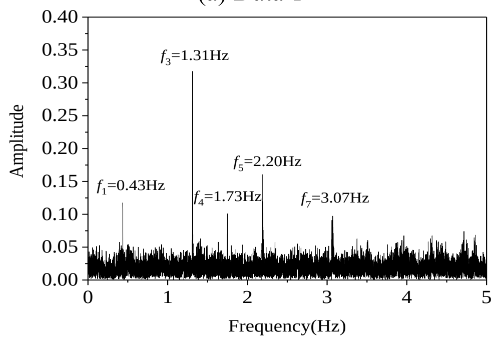

(b) Data 2

Fig. 6 Power spectral density of longitudinal acceleration

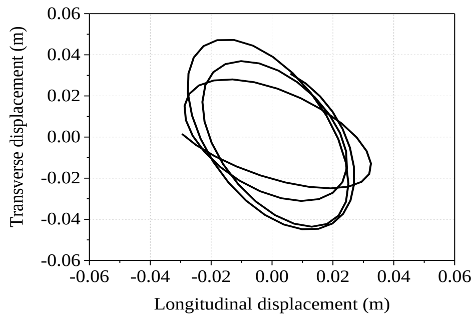

(a) Data 1

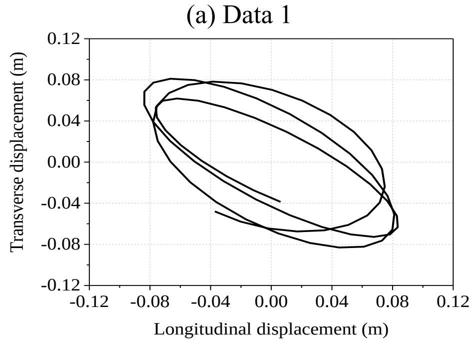

(b) Data 2

Fig. 7 Trajectory of cable A

Figure 6 shows the power spectral density (PSD) of the longitudinal acceleration of Cable A for Data 1 and 2, respectively. Noted that only the time history corresponding to large amplitude vibration is used to calculate the PSD in Fig.6. It can be observed from Fig.6 that multiple modes are involved in the hanger vibration. However, it should be pointed out that the higher frequency components of the acceleration are more obvious than those of the displacement. Figure 7 presents the trajectory of Cable A when large amplitude oscillation takes place. It could be found that the trajectory of Cable A is close to a clockwise ellipse, which agrees well with the major characteristics of wake-induced vibration (Païdoussis *et al*. 2011; Yagi *et al*. 2015).

2. Theoretical model of wake-induced vibration for 3-D continuous cable

3.1 Motion equations of the leeward cable

A 3-D continuous twin-cable hanger is considered and a coordinate system *oxyz* is defined, as shown in Fig.8, where the origin is at the top end of the leeward cable; *x* and *y* axes are respectively parallel and perpendicular to the wind direction in the horizontal plane; *z* axis is parallel to the axial direction of the leeward cable. The following assumptions are made in this study:

(1) Quasi-steady assumption is utilized to evaluate wind force on the leeward cable.

(2) The axial vibration of cable is neglected.

(3) The flexural, torsional and shear stiffness of cable are neglected.

(4) The constitutive relation of cable follows Hooke's law.

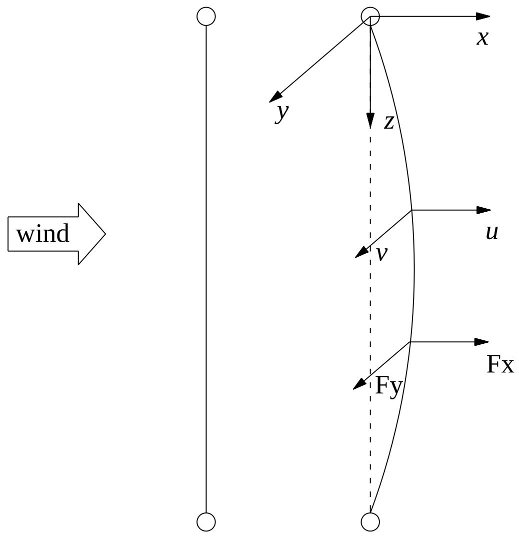

Fig. 8 3-D continuous twin-cable hanger

Accordingly, the motion equations governing the leeward cable could be expressed as,

$$\frac{\partial}{\partial z}[(T+\tau)\frac{\partial u}{\partial z}]+F_x(z,t)=M\frac{\partial^2 u}{\partial t^2}+c_1\frac{\partial u}{\partial t} \tag{1}$$

$$\frac{\partial}{\partial z}[(T+\tau)\frac{\partial v}{\partial z}]+F_y(z,t)=M\frac{\partial^2 v}{\partial t^2}+c_2\frac{\partial v}{\partial t} \tag{2}$$

where T is the static cable tension; τ is the dynamic cable tension; u and v are the dynamic displacement components in the x and y directions, respectively; $F_x(z,t)$ and $F_y(z,t)$ are the aerodynamic forces per unit length in the x and y directions, respectively; M is the cables mass per unit length; c_1 and c_2 are the linear structural damping coefficients in the x and y directions, respectively.

The dynamic tension τ could be obtained from (Irvine 1981),

$$\tau = EA\frac{dz^{*2} - dz^2}{2dz^2} \tag{3}$$

where E is the elasticity modulus of the cable; A is the area of the cross section of the cable; dz^* and dz are the lengths of the deformed and undeformed cable element, respectively. According to geometrical relationship, one have,

$$dz^{*2} = dz^2 + \partial u^2 + \partial v^2 \tag{4}$$

Substituting Equation (4) into Equation (3), one has,

$$\tau = EA\frac{\partial u^2 + \partial v^2}{2dz^2} \tag{5}$$

By using of the Equation (5), the Equations (1) and (2) can be rewritten as,

$$\begin{aligned} &T\frac{\partial^2 u}{\partial z^2} + \frac{EA}{2}[3(\frac{\partial u}{\partial z})^2\frac{\partial^2 u}{\partial z^2} + 2\frac{\partial^2 v}{\partial z^2}\frac{\partial v}{\partial z}\frac{\partial u}{\partial z} + (\frac{\partial v}{\partial z})^2\frac{\partial^2 u}{\partial z^2}] \\ &+F_x(z,t) = M\frac{\partial^2 u}{\partial t^2} + c_1\frac{\partial u}{\partial t} \end{aligned} \tag{6a}$$

$$\begin{aligned} &T\frac{\partial^2 v}{\partial z^2} + \frac{EA}{2}[3(\frac{\partial v}{\partial z})^2\frac{\partial^2 v}{\partial z^2} + 2\frac{\partial^2 u}{\partial z^2}\frac{\partial u}{\partial z}\frac{\partial v}{\partial z} + (\frac{\partial u}{\partial z})^2\frac{\partial^2 v}{\partial z^2}] \\ &+F_y(z,t) = M\frac{\partial^2 v}{\partial t^2} + c_2\frac{\partial v}{\partial t} \end{aligned} \tag{6b}$$

According to the quasi-steady assumption, the aerodynamic forces on the leeward cable, F_x and F_y, could be given by,

$$F_{x(y)}(z,t) = \frac{1}{2}\rho U^2 D C_{D(L)}(x,y) \tag{7}$$

where ρ is the air density; U is the wind velocity; D is the diameter of the cable; $C_{D(L)}(x,y)$ is the mean drag (lift) coefficients of the leeward cable. The C_D and C_L of Deng *et al.* (2019b) obtained from wind tunnel tests are adopted in this study.

3.2 Numerical solution method

The finite difference method (FDM) is adopted to numerically solve the motion equations. The leeward cable is uniformly discretized into N segments in space, as shown in Fig.9. The space node is j=0, 1, 2, …, N from the top to the bottom and the space step h equals to L/N, in which L is the length of the cable. The time node is k=0, 1, 2, …, M and the time step η equals to T_t/M, in which T_t is the total calculation time.

The second-order central difference is used and accordingly the derivatives of $\frac{\partial^2 u}{\partial z^2}$, $\frac{\partial^2 v}{\partial z^2}$, $\frac{\partial^2 u}{\partial t^2}$, $\frac{\partial^2 v}{\partial t^2}$, $\frac{\partial u}{\partial t}$ and $\frac{\partial v}{\partial t}$ in Equation (6) could be expressed as (Li *et al.* 2014),

$$\frac{\partial^2 u}{\partial z^2}\Big|_j^k = \frac{1}{h^2}(u_{j-1}^k - 2u_j^k + u_{j+1}^k) + o(h^2) \tag{8a}$$

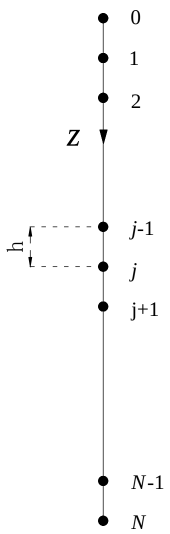

Fig. 9 Space discretization of the leeward cable

$$\frac{\partial^2 v}{\partial z^2}\Big|_j^k = \frac{1}{h^2}(v_{j-1}^k - 2v_j^k + v_{j+1}^k) + o(h^2) \tag{8b}$$

$$\frac{\partial u}{\partial z}\Big|_j^k = \frac{1}{2h}(u_{j+1}^k - u_{j-1}^k) + o(h^2) \tag{8c}$$

$$\frac{\partial v}{\partial z}\Big|_j^k = \frac{1}{2h}(v_{j+1}^k - v_{j-1}^k) + o(h^2) \tag{8d}$$

$$\frac{\partial^2 u}{\partial t^2}\Big|_j^k = \frac{1}{\eta^2}(u_j^{k-1} - 2u_j^k + u_j^{k+1}) + o(\tau^2) \tag{8e}$$

$$\frac{\partial^2 v}{\partial t^2}\Big|_j^k = \frac{1}{\eta^2}(v_j^{k-1} - 2v_j^k + v_j^{k+1}) + o(\tau^2) \tag{8f}$$

$$\frac{\partial u}{\partial t}\Big|_j^k = \frac{1}{2\eta}(u_j^{k+1} - u_j^{k-1}) + o(\tau^2) \tag{8g}$$

$$\frac{\partial v}{\partial t}\Big|_j^k = \frac{1}{2\eta}(v_j^{k+1} - v_j^{k-1}) + o(\tau^2) \tag{8h}$$

where u_j^k and v_j^k represent the values of u and v at space node j and time node k, respectively.

Substituting Equation (8) into Equation (6), difference scheme can be obtained,

$$\begin{aligned} u_j^{k+1} = &\frac{1}{(\frac{M}{\eta^2} + \frac{c_1}{2\eta})}\{\frac{T}{h^2}(u_{j-1}^k - 2u_j^k + u_{j+1}^k) \\ &+\frac{EA}{2h^4}[\frac{3}{4}(u_{j+1}^k - u_{j-1}^k)^2(u_{j-1}^k - 2u_j^k + u_{j+1}^k) \\ &+\frac{1}{2}(v_{j-1}^k - 2v_j^k + v_{j+1}^k)(u_{j+1}^k - u_{j-1}^k)(v_{j+1}^k - v_{j-1}^k) \\ &+\frac{1}{4}(v_{j+1}^k - v_{j-1}^k)^2(u_{j-1}^k - 2u_j^k + u_{j+1}^k)] \\ &+(\frac{c_1}{2\eta} - \frac{M}{\eta^2})u_j^{k-1} + \frac{2M}{\eta^2}u_j^k + F_x(z_j,t_k)\} \end{aligned} \qquad (9a))$$

(j =1,2,3,……,N-1, k=1,2,3,4,……M)

$$
\begin{aligned}
v_j^{k+1} = & \frac{1}{(\frac{M}{\eta^2}+\frac{c_1}{2\eta})}\{\frac{T}{h^2}(v_{j-1}^k-2v_j^k+v_{j+1}^k) \\
& +\frac{EA}{2h^4}[\frac{3}{4}(v_{j+1}^k-v_{j-1}^k)^2(v_{j-1}^k-2v_j^k+v_{j+1}^k) \\
& +\frac{1}{2}(u_{j-1}^k-2u_j^k+u_{j+1}^k)(u_{j+1}^k-u_{j-1}^k)(v_{j+1}^k-v_{j-1}^k) \\
& +\frac{1}{4}(u_{j+1}^k-u_{j-1}^k)^2(v_{j-1}^k-2v_j^k+v_{j+1}^k)] \\
& +(\frac{c_1}{2\eta}-\frac{M}{\eta^2})v_j^{k-1}+\frac{2M}{\eta^2}v_j^k+F_y(z_j,t_k)\}
\end{aligned}
\tag{9b}
$$

(j =1,2,3,……,N-1, k=1,2,3,4,……M)

The boundary and initial conditions should be given before the Equations (9) is solved. The boundary and initial conditions could be expressed as follows,

$$
\begin{cases}
u(0,t)=v(0,t)=0 \qquad u(L,t)=v(L,t)=0 \qquad t\in(0,T) \\
u(x,0)=v(x,0)=0 \qquad \dfrac{\partial u(x,0)}{\partial t}=\dfrac{\partial v(x,0)}{\partial t}=0 \qquad x\in(0,L)
\end{cases}
\tag{10}
$$

4. Numerical example

The No. 2 hanger of the Xihoumen Bridge is taken as the background for the numerical simulation. The cable length is L=160m; the static cable tension is T=495.8kN; the mass per unit length is M=31kg/m; the diameter of the cable D=0.088 m; the elasticity modulus is E=1.1×10^{11} N/m^2; the structural damping ratios for the first mode in the x and y directions, ξ_x and ξ_y, are both 0.1%. In this numerical example, the terrain category A stipulated in Chinese Code, which has an exponent of 0.12, is adopted to consider the increase of wind speed with the height. The wind velocity at the height of bridge deck is U_{ref}=8m/s. The detailed parameters used in the numerical example are summarized in Tab.1. The numerical simulations are conducted within the spatial range of 4≤X≤10 and 0≤Y≤4 with a uniform interval of ΔX=ΔY=0.25. Accordingly, there are 425 computational cases in total.

4.1 Cable responses

Figure 10 presents the spatial distributions of the maximum one-side resultant amplitude (A_{max}/D) of the stable vibration at the mid-point and quarter-point of the leeward cable, respectively. It can be found from Fig.10 that obvious oscillation of the leeward cable could be observed within the spatial region of 0.25≤Y≤1.75. The amplitudes at the mid-point of the leeward cable are larger than those at the quarter-point and the maximum amplitude, about 1.66D, occurs at the point of X=5.75 and Y=0.25. It is noted that the spatial position of the No. 2 hanger of the Xihoumen Bridge shown in Fig. 4 and Fig.5 is about X=6.8 and Y=0.60.

Figure 11 presents the time histories of displacements at the mid-point of the leeward cable for four typical cases (X=5.5, Y=0.25; X=5.5, Y=1; X=8, Y=0.25 and X=9.5, Y=0.25). It can be found from Fig.11 that the oscillation amplitude of the leeward cable in the along-wind direction

Table1 Calculation parameters

Parameters	Symbol	Value
Length (m)	L	160
Static cable tension (kN)	T	495.8
Mass per unit length (kg/m)	M	31
Diameter of the cable (m)	D	0.088
Elasticity modulus (N/m^2)	E	1.1×10^{11}
Wind velocity (m/s)	U_{ref}	8
Damping ratio	ξ_x, ξ_y	0.001

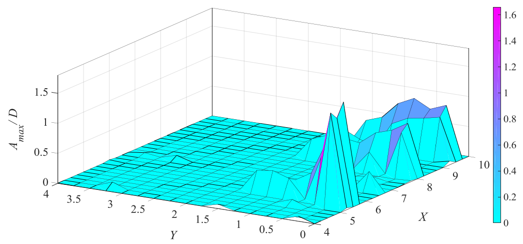

(a)Mid-point of the leeward cable

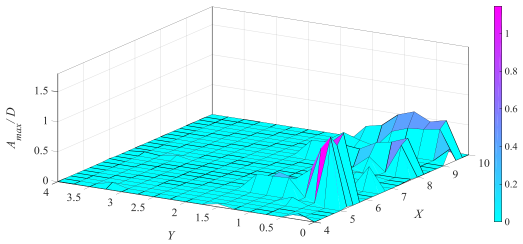

(b) Quarter-point of the leeward cable

Fig. 10 Spatial distribution of the one-side amplitude of the leeward cable

is much larger than that in the cross-wind direction. The stable trajectories at the mid-point of the leeward cable are shown in Fig.12. It can be observed from Fig.12 that the stable trajectory of the leeward cable is an ellipse, which also agrees well with the results obtained from the field observations (as shown in Fig.7). Furthermore, the direction of the dominant axis in Fig.12 is almost the same as the wind tunnel results obtained by Yagi *et al*. (2015). It should be noted that two dampers have been installed between the cables of the No. 2 hanger during the field measurements.

Figure 13 presents the PSD of the stable vibration at 1/10 span point of the leeward cable for the two typical cases (X=5.5, Y=0.25; X=5.5, Y=1) obtained from numerical simulations. As can be seen from Fig.13, the first several modes (up to the 5th mode) could be evoked in the wake-induced vibration obtained from numerical simulation and the amplitude of the first mode is obviously larger than those of the rest modes. Compared with the PSD of the responses obtained from field observations (as indicated in Fig.6), the highest mode evoked in the vibration (up to the 5th mode) is lower than that obtained from field observations (up to the 11th mode). The main reason is that the response obtained from numerical simulations is only induced by wake-induced vibration. However, the response obtained from field observations may results from many

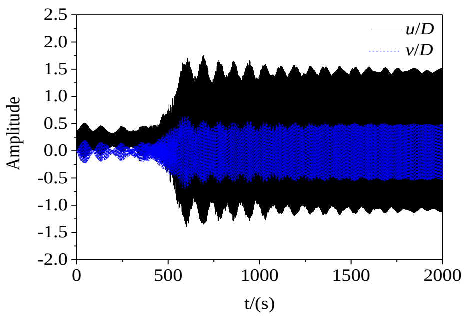

(a) *X*=5.5, *Y*=0.25

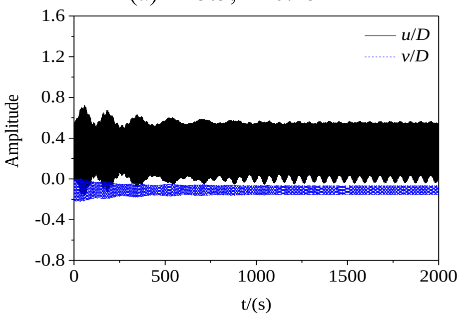

(b) *X*=5.5, *Y*=1

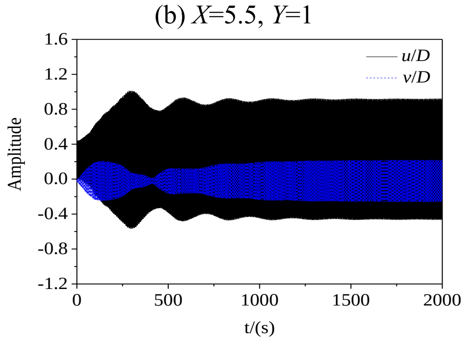

(c) *X*=8, *Y*=0.25

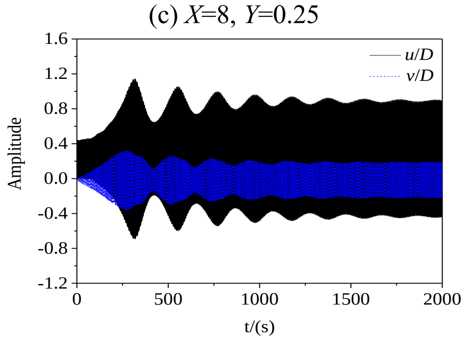

(d) *X*=9.5, *Y*=0.25

Fig. 11 Time histories of the displacements at the mid-point of the leeward cable

other factors besides wake-induced vibration, such as vortex-induced vibration and buffeting. Fig.14 shows the oscillation shapes of the leeward cable at the calculation time of *t*=1000s, 1250s, 1500s, 1750s and 2000s for the two typical cases (*X*=5.5, *Y*=0.25; *X*=5.5, *Y*=1) obtained from numerical simulations. It could be found from Fig.14 that the oscillation shapes of leeward cable obtained from numerical simulations changes with the variation of the time. It appears that the oscillation shape at the time of *t*=2000s mainly comes from the first mode shape for the two typical cases.

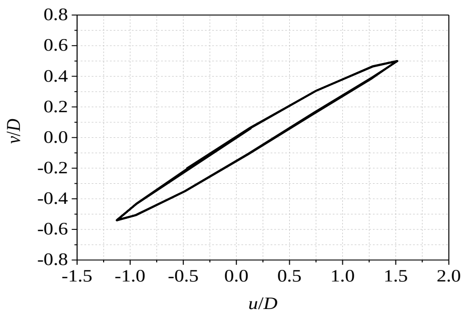

(a)*X*=5.5, *Y*=0.25

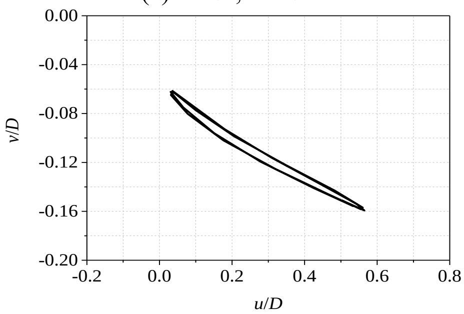

(b) *X*=5.5, *Y*=1

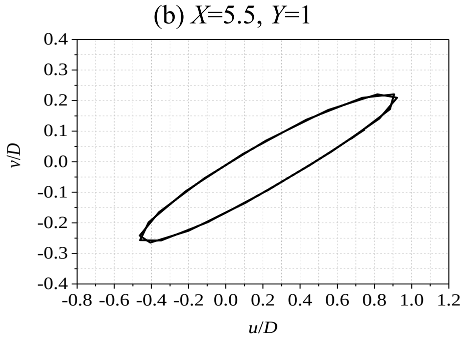

(c) *X*=8, *Y*=0.25

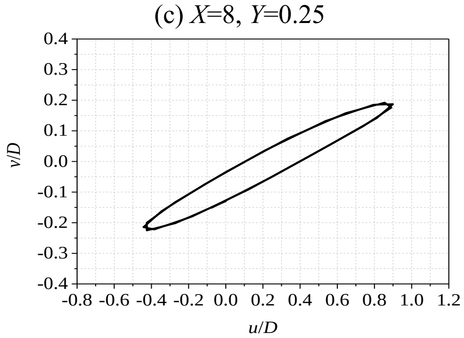

(d) *X*=9.5, *Y*=0.25

Fig. 12 Stable trajectory at the mid-point of the leeward cable

Based on the results obtained from numerical simulations, the main features of the observed responses of the hangers of the Xihoumen Bridge are reproduced. Hence, the wake-induced vibration might be the underlying mechanism of the vibration of the hangers of the Xihoumen Bridge.

4.2 Effect of the structural damping

To mitigate the wind-induced vibrations of the hangers of the Xihoumen Bridge, dampers were installed between the cables of the hanger from the construction stage. The field tests show that the modal damping ratio of the cable could be reached about 1.5%. The vibrations of the hangers

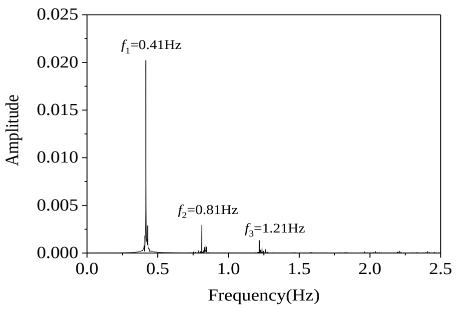

(a)Along-wind (X=5.5, Y=0.25)

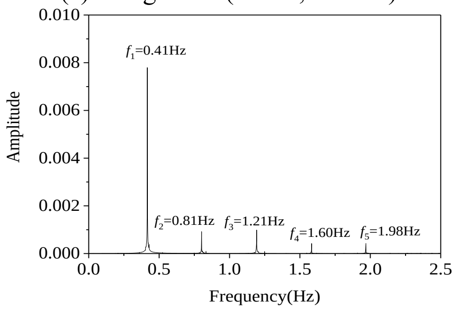

(b) Cross-wind (X=5.5, Y=0.25)

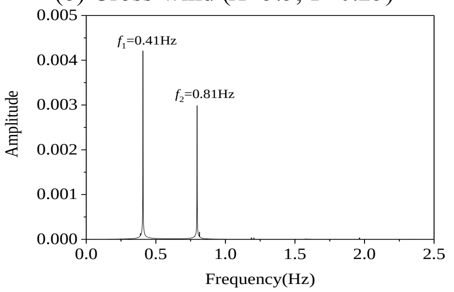

(c) Along-wind (X=5.5, Y=1)

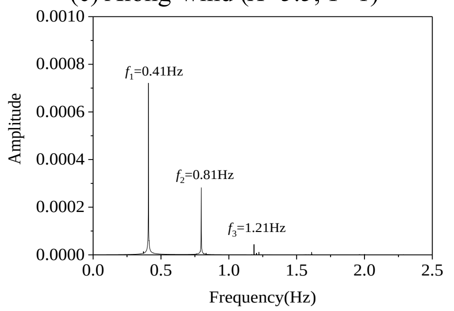

(d) Cross-wind (X=5.5, Y=1)

Fig. 13 PSD of the stable vibration at 1/10 span point of the leeward cable obtained from numerical simulations

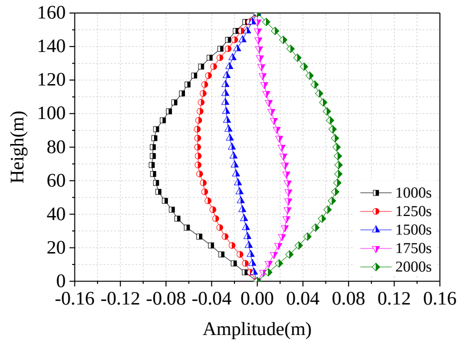

(a)Along-wind (X=5.5, Y=0.25)

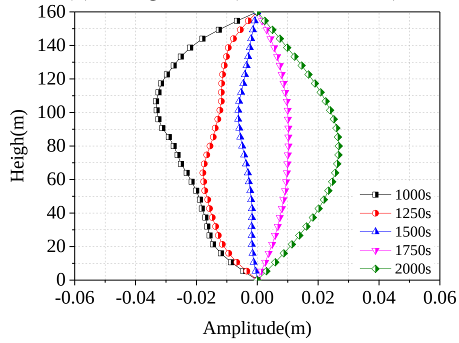

(b) Cross-wind (X=5.5, Y=0.25)

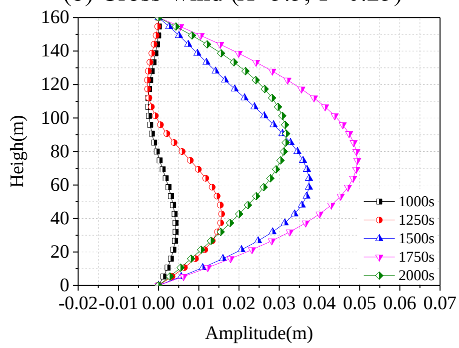

(c) Along-wind (X=5.5, Y=1)

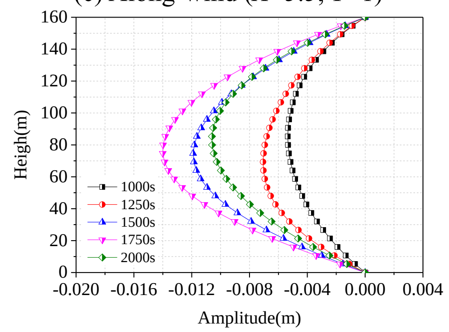

(d) Cross-wind (X=5.5, Y=1)

Fig. 14 Oscillation shapes of the leeward cable obtained from numerical simulations

on the Xihoumen Bridge are unfortunately not effectively suppressed, while the vibration of stay cable on cable-stayed bridges could be well mitigated at the damping ratio level of 0.5% (Chen *et al*. 2002; Li *et al*. 2014). Fig.15 shows the relationship between the amplitude at the mid-point of the leeward cable and the damping ratio for the typical case of X=5.5, Y=1.25 obtained from the numerical simulations. It can be found from Fig.15 that the along-wind amplitude of the cable slowly decreases with the damping ratio when it is lower than 1.5%. However, the cross-wind amplitude of the cable keeps almost unchanged within the damping ratio range of 0.1%~1.5%. This observation indicates that it is not an optimal countermeasure to mitigate the wake-induced vibration of the hangers by increasing the structural damping. Deng *et al*. (2019a) found that the wake-induced vibration is evoked because of the negative aerodynamic stiffness and suggested that the increase of cable stiffness may be a more effective countermeasure to mitigate the wake-induced vibration of the hangers. In fact, spacers were installed on the hangers of the Xihoumen Bridge in the summer of 2015 and the wake-induced vibration seems to be well mitigated from then on.

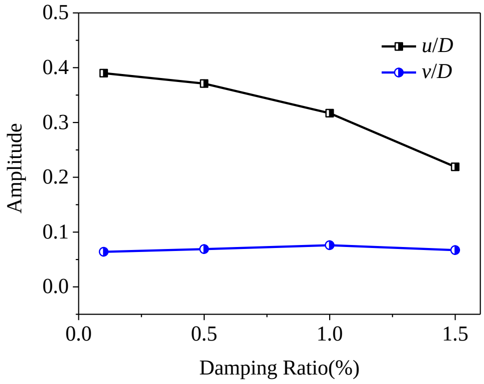

Fig. 15 Relationship between the amplitudes at mid-point of the cable and the damping ratios

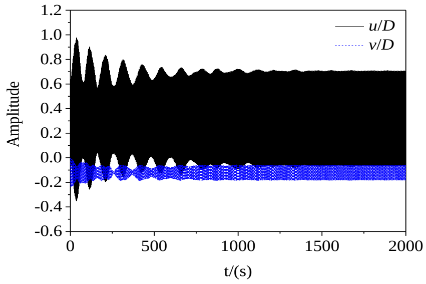

(a) $\xi = 0.1\%$

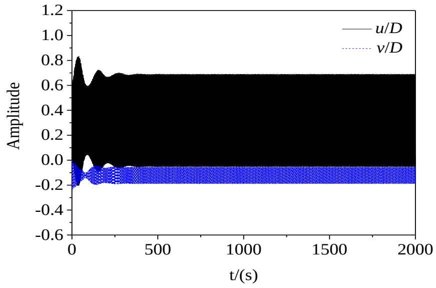

(b) $\xi = 0.5\%$

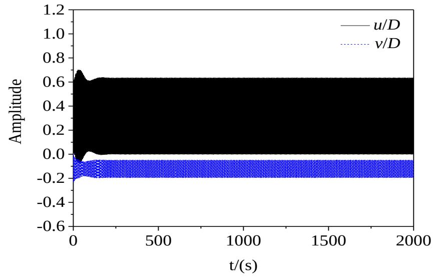

(c) $\xi = 1\%$

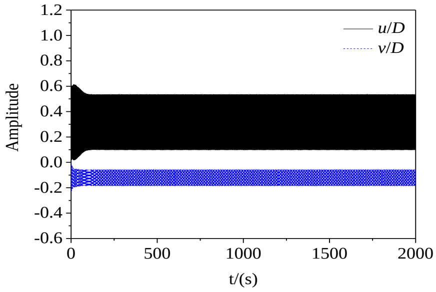

(d) $\xi = 1.5\%$

Fig. 16 Time histories of displacements at mid-point of the leeward cable for various damping ratios (X=5.5, Y=1.25)

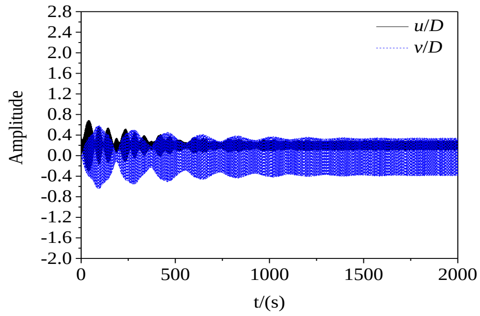

(a) X=5.5, Y=0.25

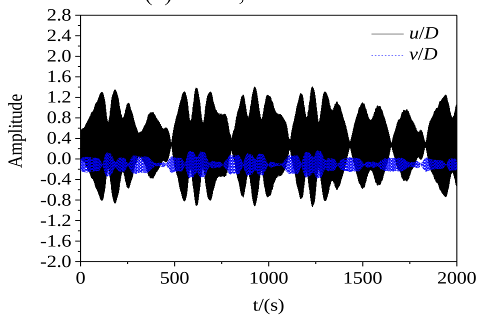

(b) X=5.5, Y=1

Fig. 17 Time histories of the displacements at the mid-point of the leeward cable (a_w=0.5D)

Figure 16 presents the time histories of the displacements at the mid-point of the leeward cable for various damping ratios for the case of X=5.5, Y=1.25. It can be found from Fig.16 that the amplitude of the cable in the along-wind direction slowly decreases with the damping ratio. However, the amplitude in the cross-wind direction seems to be less sensitive to the damping ratio.

4.3 Effect of the windward cable vibration

The field measurements show that obvious along-wind vibration of the windward cable could be found together with the large amplitude vibration of the leeward cable, as described in Fig.5 (b) and (d). Hence, the windward cable vibration might be important to be considered for the leeward cable vibration. In this study, the along-wind vibration of the windward cable is simply assumed as,

$$u_w(z) = a_w \sin \omega_w t \tag{11}$$

where a_w is the maximum one-side amplitude of the windward cable; ω_w is the vibration frequency, equals to the first natural frequency of the cable. The aerodynamic forces of the leeward cable (Equation (7)) are obtained in consideration of Equation (11).

Figures 17-19 present the time histories of the displacements at the mid-point of the leeward cable for various values of a_w = 0.5D, 1.0D and 1.5D for the two typical cases (X=5.5, Y=0.25 and X=5.5, Y=1). From Figs. 17-19, it can be seen that the amplitude of the leeward cable obviously increases with the increase of the amplitude of the windward cable a_w. Therefore, the large amplitude vibration of windward cable can facilitate the vibration of leeward cable in the aerodynamic interference, which is consistent with the existing experimental results (Kim *et al.* 2009; Armin *et al.* 2018).

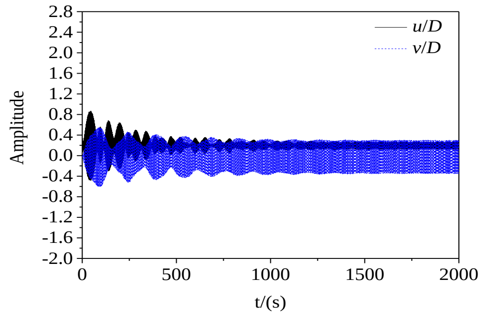

(a) X=5.5, Y=0.25

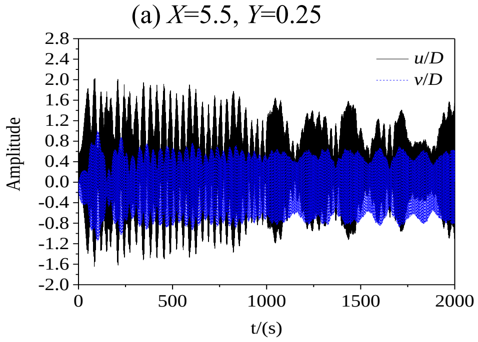

(b) X=5.5, Y=1

Fig. 18 Time histories of the displacements at the mid-point of the leeward cable (a_w=1.0D)

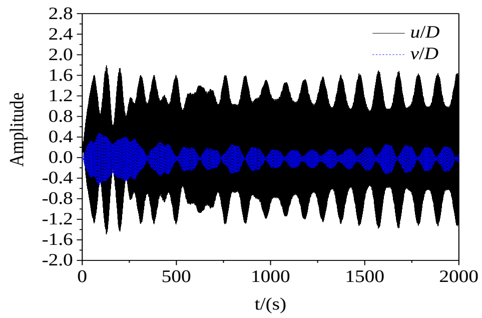

(a)X=5.5, Y=0.25

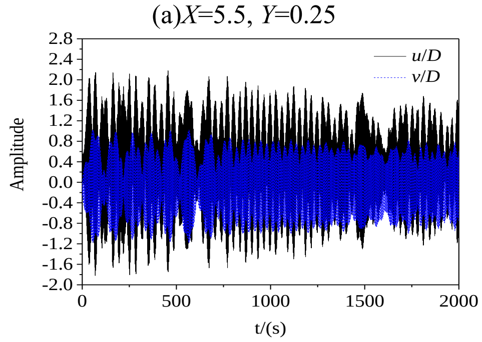

(b) X=5.5, Y=1

Fig. 19 Time histories of the displacements at the mid-point of the leeward cable (a_w=1.5D)

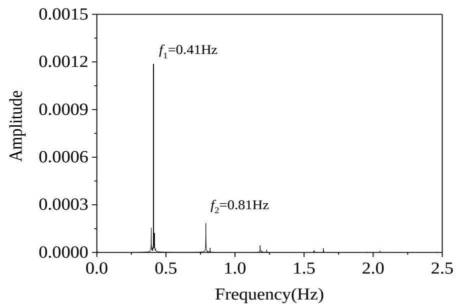

(a)Along-wind (X=5.5,Y=0.25)

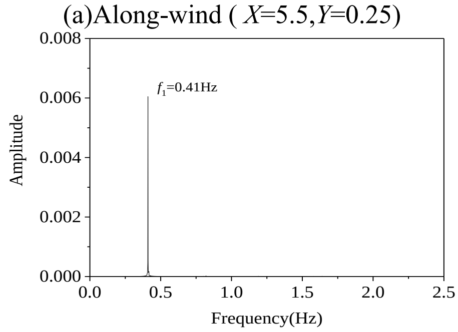

(b) Cross-wind (X=5.5,Y=0.25)

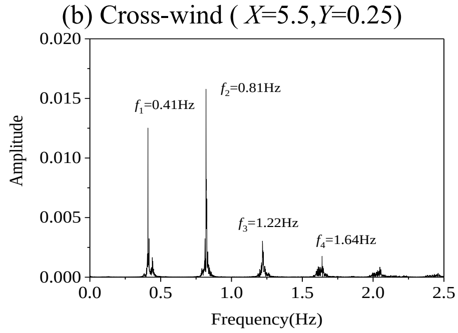

(c) Along-wind (X=5.5, Y=1)

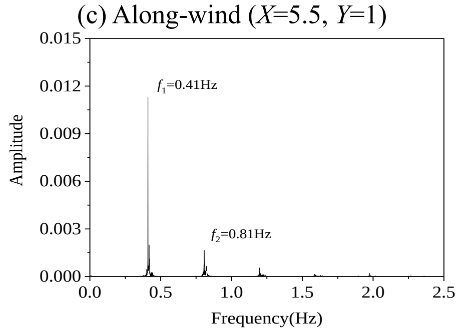

(d) Cross-wind (X=5.5, Y=1)

Fig. 20 PSD of the stable vibration at 1/10 span point of the leeward cable obtained from numerical simulations (a_w=1.0D)

Figure 20 presents the PSD of the stable vibration at 1/10 span point of the leeward cable for the cases of X=5.5, Y=0.25 and X=5.5, Y=1 for a_w=1.0D. Although some higher model frequencies are found in the vibration, the leeward cable vibration is dominated by the first model frequency. This observation is similar to that in the case of fixed windward cable. The stable trajectories at the mid-point of the leeward cable are shown in Fig.21. It could be found that the trajectory of leeward is also close to an ellipse.

5. Concluding Remarks

The underlying mechanism of the wind-induced vibration of the hangers of the Xihoumen Bridge was investigated in this study based on the field measurements and theoretical analyses. First, a series of field observations on the No. 2 hanger of the Xihoumen Bridge was carefully conducted and large amplitude vibration of the hanger were found. The wind direction when the hanger oscillated violently was 170º, which was nearly perpendicular to the beam of the Xihoumen Bridge and the wind velocity was

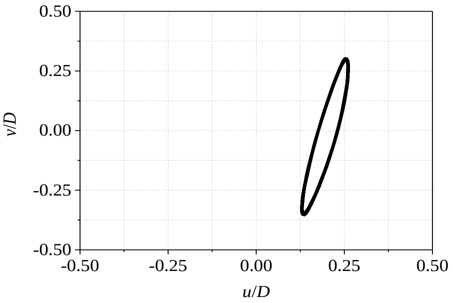

(a)X=5.5, Y=0.25

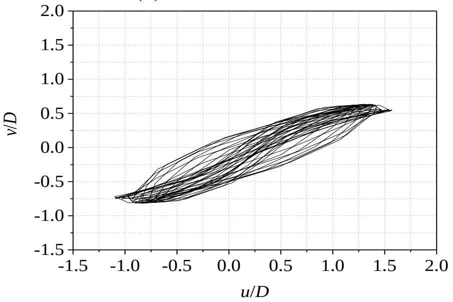

(b) X=5.5, Y=1

Fig. 21 Stable trajectory at the mid-point of the leeward cable (a_w=1.0D)

about 6 m/s. The oscillation amplitude of the leeward cable was obviously larger than that of the windward cables. Furthermore, the trajectory of the cable is close to a clockwise ellipse, which agreed well with the major characteristics of wake-induced vibration. Then, a theoretical model for the wake-induced vibration based on a 3-D continuous cable was established to numerically study the underlying mechanism of the hanger vibration. The motion equations of the continuous leeward cable were derived and the aerodynamic forces acting on the cable is obtained by using quasi-steady assumption. The finite difference method (FDM) was adopted to obtain the vibration responses of the leeward cable. Finally, numerical simulations by using the structural parameters of the No.2 hanger of the Xihoumen Bridge were carried out within the spatial range of $4 \le X \le 10$ and $0 \le Y \le 4$ with a uniform interval of $\Delta X = \Delta Y = 0.25$. The results showed that obvious oscillations of the leeward cable occured in the spatial region of $0.25 \le Y \le 1.75$, in which the maximum one-side resultant amplitude (A_{max}/D) at mid-point of cable could reach 1.66D at the point of X=5.75 and Y=0.25. Moreover, the stable trajectory of the leeward cable was an ellipse. The results obtained from numerical simulations agreed well with the main features obtained from the field observation on the Xihoumen Bridge. Hence, the wake-induced vibration might be the underlying mechanism of the vibration of the hangers of the Xihoumen Bridge. The effects of damping ratio on the wake-induced vibration of the leeward cable were numerically analyzed. The results showed that the amplitude of the cable slowly decreases with the damping ratio when the damping ratio is lower than 1.5%. It is noted that the required damping ratio to substantially suppress the wake-induced vibration of the hangers on the suspension bridges is as high as 1.5%, which is far larger than that for the vibration mitigation of the stay cables on the cable-stayed bridges. Moreover, it was found that the large amplitude vibration of windward cable can facilitate the leeward cable oscillation in the wake-induced vibration.

Acknowledgments

This study is jointly supported by the National Natural Science Foundation of China (51578234) and the National Basic Research Program of China (2015CB057702) and Hunan Provincial Innovation Foundation For Postgraduate (CX20190290) and those supports are greatly appreciated by the authors.

References

Akosile, O.O. and Sumner, D. (2003), "Staggered circular cylinders immersed in a uniform planar shear flow", *J. Fluids Struct.*, **18**, 613-633. https://doi.org/10.1016/j.jfluidstructs.2003.07.014.

Alam, M.M., Moriya, M., Takai, K. and Sakamoto, H. (2003), "Fluctuating fluid forces acting on two circular cylinders in a tandem arrangement at a subcritical Reynolds number", *J. Wind Eng. Industrial Aerodynam.*, **91**, 139-154. https://doi.org/10.1016/S0167-6105(02)00341-0.

Arie, M., Kiya, M., Moriya, M. and Mori, H. (1983), "Pressure fluctuations on the surface of two circular cylinders in tandem arrangement", *J. Fluid. Eng.*, **105**, 161-167. https://doi.org/10.1115/1.3240956.

Armin, M., Khorasanchi, M. and Day, S. (2018), "Wake interference of two identical oscillating cylinders in tandem: An experimental study", *Ocean Eng.*, **166**, 311-323. https://doi.org/10.1016/j.oceaneng.2018.08.012.

Assi, G. R. S. (2014), "Wake-induced vibration of tandem cylinders of different diameters", *J. Fluids Struct.*, **50**, 329-339. https://doi.org/10.1016/j.jfluidstructs.2014.07.001.

Assi, G. R. S., Bearman, P. W. and Meneghini, J. R. (2010), "On the wake-induced vibration of tandem circular cylinders: the vortex interaction excitation mechanism", *J. Fluid. Mech.*, **661**(4), 365-401. https://doi.org/10.1017/S0022112010003095.

Assi, G.R.S., Bearman, P.W., Carmo, B.S., Meneghini, J.R., Sherwin, S.J. and Willden, R.H.J. (2013), "The role of wake stiffness on the wake-induced vibration of the downstream cylinder of a tandem pair", *J. Fluid. Mech.*, **718**(3), 210-245. https://doi.org/10.1017/jfm.2012.606.

Chen, W. L., Gao, D. L., Li, H. and Hu, H. (2018), "Wake-flow-induced vibrations of vertical hangers behind the tower of a long-span suspension bridge", *Eng. Struct.*, **169**, 188-200. https://doi.org/10.1016/j.engstruct.2018.05.049.

Chen, Z. Q., Lei, X., Hua, X. G., Li, S. Y., Yan, Y. X., Wen, Q. and Niu H. W. (2016), "Research and application of vibration control method for hanger cables in long-span suspension bridge", *J. Hunan University (Natural Science)*, **43**(1), 1-10.

Deng, Y. C., Li, S. Y. and Chen, Z. Q. (2019a), "Unsteady theoretical analysis on the wake-induced vibration of the hangers of suspension bridges", *J. Bridge Eng.*, https://doi.org/10.1061/(ASCE)BE.1943-5592.0001339.

Deng, Y. C., Li, S. Y., Yan, J. T. and Chen, Z. Q. (2019b), "A Comparative Study on the Aerodynamic Stability of Two Kinds of Hanger of Suspension Bridge", *China Civi Eng. J.,* **52**(1), 82-88.

Du, X. Q., Zhao, Y., Chen, S. R., Daichin and Jiang. B. J. (2017), "Effects of surface roughness on wake-induced vibrations of two parallel cables", *9th Asia-Pacific Conference on Wind*

Engineering, Auckland, New Zealand, December.
Fujino, Y., Kimura, K. and Tanaka, H. (2012), *Wind Resistant Design of Bridges in Japan: Developments and Practices*, Springer, New York.
Greco, F., Lonetti, P. and Pascuzzo, A. (2013), "Dynamic analysis of cable-stayed bridges affected by accidental failure mechanisms under moving loads", *Math. Problems Eng.,* https://doi.org/10.1155/2013/302706.
Gu, Z. F. and Sun, T. F. (1999), "On interference between two circular cylinders in staggered arrangement at high subcritical Reynolds numbers", *J. Wind Eng. Industrial Aerodynam.*, **80**, 287-309. https://doi.org/10.1016/S0167-6105(98)00205-0.
Hua, X. G., Chen, Z. Q., Lei, X., Wen, Q. and Niu, H. W. (2019), "Monitoring and control of wind-induced vibrations of hanger ropes of a suspension bridge", *Smart Struct. Syst.*, **23**(6), 125-141. https://doi.org/10.12989/sss.2019.23.6.683.
Igarashi, T. (1981), "Characteristics of the flow around two circular cylinders arranged in tandem (1st report)", *Bullet. JSME*, **24**, 323-331. https://doi.org/10.1299/jsme1958.24.323.
Igarashi, T. (1984), "Characteristics of the flow around two circular cylinders arranged in tandem (second report, unique flow phenomenon at small spacing)", *Bullet. JSME*, **27**, 2380-2387. https://doi.org/10.1299/jsme1958.27.2380.
Irvine, H. M. (1981), *Cable Structure*, The MIT Press, Cambridge, Massachusetts and London, United Kingdom.
Kim, S., Alam, M. M., Sakamoto, H. and Zhou, Y. (2009), "Flow-induced vibrations of two circular cylinders in tandem arrangement. part 1: characteristics of vibration", *J. Wind Eng. Industrial Aerodynam.*, **97**(5), 304-311. https://doi.org/10.1016/j.jweia.2009.07.004.
Laursen, E., Bitsch, N. and Andersen, J. E. (2005), "Analysis and mitigation of large amplitude cable vibrations at the Great Belt East Bridge", *IABSE Symposium Report*, **91**(3), 64-71.
Li, Y. L., Tang, H. J., Lin, Q. M.,and Chen, X. Z. (2017), "Vortex-induced vibration of suspenders in the wake of bridge tower by numerical simulation and wind tunnel test", *J. Wind Eng. Industrial Aerodynam.*, **164**, 164-173. https://doi.org/10.1016/j.jweia.2017.02.017.
Li, S. Y., Chen, Z. Q. and Li, S. K., (2014), "Theoretical investigation on rain-wind induced vibration of a continuous stay cable with given rivulet motion", *Wind Struct.*, **19**(5), 481-503. http://dx.doi.org/10.12989/was.2014.19.5.481.
Li, S.Y., Xiao, C.Y., Wu, T. and Chen, Z.Q. (2019), "Aerodynamic interference between the cables of the suspension bridge hanger", *Adv. Struct. Eng.*, **19**(5), 481-503. https://doi.org/10.1177/1369433218820623.
Lonetti, P. and Pascuzzo, A. (2014), "Vulnerability and failure analysis of hybrid cable-stayed suspension bridges subjected to damage mechanisms", *Eng. Failure Anal.*, **45**, 470-495. https://doi.org/10.1016/j.engfailanal.2014.07.002.
Lonetti, P., F., Pascuzzo, A. and Davanzo, A. (2016). "Dynamic Behavior of Tied-Arch Bridges under the Action of Moving Loads", *Math. Problems Eng.*, http://dx.doi.org/10.1155/2016/2749720
Mysa, R. C., Kaboudian, A. and Jaiman, R. K. (2016), "On the origin of wake-induced vibration in two tandem circular cylinders at low Reynolds number", *J. Fluids Struct.*, **61**, 76-98. https://doi.org/10.1016/j.jfluidstructs.2015.11.004.
Mysa, R. C., Law, Y. Z. and Jaiman, R. K. (2017), "Interaction dynamics of upstream vortex with vibrating tandem circular cylinder at subcritical Reynolds number", *J. Fluids Struct.*, **75**, 27-44. https://doi.org/10.1016/j.jfluidstructs.2017.08.001.
Païdoussis, M. P., Price, S. J. and Langre, E. D. (2011), *Fluid-Structure Interactions: Cross-flow-induced Instabilities*, Cambridge University Press, United Kingdom.
Qin, B., Alam, M. M., Ji, C., Liu, Y. and Xu, S. (2018), "Flow-induced vibrations of two cylinders of different natural frequencies", *Ocean Eng.*, **155**, 189-200. https://doi.org/10.1016/j.oceaneng.2018.02.048.
Sumner, D., Price, S. J. and Païdoussis, M. P. (2000), "Flow-pattern identification for two staggered circular cylinders in cross-flow", *J. Fluid. Mech.*, **411**(411), 263-303. https://doi.org/10.1017/S0022112099008137.
Sumner, D. and Richards, M.D. (2003), "Some vortex-shedding characteristics of the staggered configuration of circular cylinders", *J. Fluids Struct.*, **17**, 345-350. https://doi.org/10.1016/S0889-9746(02)00145-7.
Sumner, D., Richards, M.D. and Akosile, O.O. (2005), "Two staggered circular cylinders of equal diameter in cross-flow", *J. Fluids Struct.*, **20**, 255-276. https://doi.org/10.1016/j.jfluidstructs.2004.10.006.
Wen, Q., Hua, X. G., Chen, Z. Q. and Niu, H. W. (2018), "Experimental study of wake-induced instability of coupled parallel hanger ropes for suspension bridges", *Eng. Struct.*, **167** (15), 175-187. https://doi.org/10.1016/j.engstruct.2018.04.023.
Yagi, T., Arima, M., Araki, S., Ogawa, S., Kosugi, T., Zain, M. R. M. and Shirato, H. (2015), "Investigation on wake-induced instabilities of parallel circular cylinders based on unsteady aerodynamic forces", *14th International Conference on Wind Engineering-Porto Alegre*, Brazil.
Zdravkovich, M.M. (1987), "The effects of interference between circular cylinders in cross flow", *J. Fluids Struct.*, **1**, 239-261. https://doi.org/10.1016/S0889-9746(87)90355-0.
Zhang, H. and Melbourne, W.H. (1992), "Interference between two circular cylinders in tandem in turbulent flow", *J. Wind Eng. Industrial Aerodynam.*, **41**(1-3), 589-600. https://doi.org/10.1016/0167-6105(92)90468-P.
Zhang, Z. T., Wu, X. B., Chen, Z. Q. and Ge, Y. J. (2016), "Mechanism of hanger oscillation at suspension bridges: buffeting-induced resonance", *J. Bridge Eng.*, **21**(3), 04015066. https://doi.org/10.1061/(ASCE)BE.1943-5592.0000834.

PL